20:1 Projection Soft X-ray Lithography Using Tri-level Resist

T. E. Jewell,* M. M. Becker,+ J. E. Bjorkholm,+ J. Bokor,+ L. Eichner,+ R. R. Freeman,+
W. M. Mansfield,+ A. A. MacDowell,# M. L. O'Malley,+ E. L. Raab,* W. T. Silfvast,% L. H. Szeto,+
D. M. Tennant,+ W. K. Waskiewicz,* D. L. White,* D. L. Windt,*° and O. R. Wood, II+

AT&T Bell Laboratories

J. H. Bruning

GCA Tropel Division
Fairport, New York 14450

ABSTRACT

We demonstrate nearly diffraction limited printing using soft x-ray radiation of approximately 36 and 14 nm wavelength. As an imaging system we used a 20×-reduction Schwarzschild-type objective with iridium coated mirrors for use at 36 nm and Mo/Si multilayer coated mirrors for use at 14 nm. An off-axis aperture and illumination were used to eliminate the central obscuration in the imaging system caused by the primary mirror. Two types of masks were used for exposures: an open-stencil one for 36 nm and a silicon membrane with a Ge absorber for 14 nm. The high absorption of carbon-based polymers at these wavelengths requires that imaging resist be very thin. Thin resist layers are not robust and, by themselves, not very useful for processing. By incorporating them into a tri-level resist, however, we have exposed, developed, and transferred features as small as 0.1 μm into silicon.

1. INTRODUCTION

Optical projection lithography has demonstrated a resolution capability of 0.35-0.5 μm.[1-3] It is anticipated that 0.25 μm resolution can be achieved using either high numerical aperture (NA) lenses at 248 nm wavelength (KrF excimer laser) or reducing the wavelength of the illumination source to 193 nm (ArF excimer laser).

One way to achieve results below 0.25 μm is to use an optical projection system with numerical aperture greater than 0.5. However, aberration correction becomes increasingly difficult requiring greater lens complexity. Thus, the residual aberrations, reduced depth of focus, and manufacturing complexity largely offset the benefits of better resolution due to increased NA. Another way to improve resolution is to decrease the wavelength below 193 nm. However, very few materials have significant transmission below 193 mm, and many of those that do, have undesirable fabrication properties. Thus, the resolution limit of optical/UV lithography appears to be about 0.25 μm.

Proximity x-ray steppers using either synchrotron radiation or plasma-generated x-rays have demonstrated the ability to print 0.5 μm features.[4-6] For these systems the resolution may be

----

* Murray Hill, New Jersey 07974
+ Holmdel, New Jersey 07733
# NSLS, Brookhaven National Laboratory, Upton, New York 11973
% Present address: University of Central Florida, Orlando, Florida 32826
° Also at the University of Maryland, College Park, Maryland 20742

Downloaded From: http://spiedigitallibrary.org/ on 03/31/2016 Terms of Use: http://spiedigitallibrary.org/ss/TermsOfUse.aspx

improved, perhaps to 0.2 μm, with appropriate selection of the wavelength and the gap between the mask and the wafer. However, because the mask used in proximity x-ray lithography must be constructed on a thin membrane, it is fragile, dimensionally unstable, difficult to fabricate, and for small mask to wafer gap there is always chance of mechanical damage. In addition, because it is 1:1 process, it requires a higher resolution mask fabrication technology than is necessary for reduction projection systems.

The prospect of extending optical imaging techniques into the soft x-ray region of the spectrum has intrigued researchers in several fields for many years. Recently, advances in optical surface fabrication and multilayer coating technology have yielded improved techniques for soft x-ray imaging: for example Walker, et al.[7] have demonstrated the use of a soft x-ray telescope for studies of the sun at 17.3 nm; several groups[8] have employed x-ray imaging for high resolution x-ray microscopy; and Kinoshita, et al.[9] have used soft x-rays at 12.4 nm to demonstrate 8× reduction projection lithography with a resolution of approximately 0.5 μm. The advantages of projection lithography over proximity lithography for the printing of features with resolution below 0.2 μm have been described by several authors.[9,10] In particular, the difficulties of producing a 1:1 transmission mask as needed for proximity printing can be avoided by using a reflective mask.[9-11]

In this paper we report the results of several experiments which have demonstrated reduction imaging at both 36 and 13.9 nm. We used undulator radiation from a synchrotron storage ring and a Schwarzschild-type all reflective objective. With iridium coated optics and 36 nm radiation we recorded 0.2 μm features at 20× reduction from an open-stencil transmission mask. Then, by using the same source tuned to 13.9 nm and objective mirrors coated with Mo/Si multilayers, we were able to print features as small as 0.1 μm from a silicon membrane transmission mask. The demonstrated resolution is close to diffraction-limited for the numerical apertures and wavelengths employed. These experiments further support the possibility that soft x-ray projection lithography may be feasible, provided that several technical issues can be successfully confronted.

2. OPTICAL SYSTEM

The 20× Schwarzschild objective used in our experiments is schematically shown in Figure 1, and it is commercially available.[12] It is a well known system of two nearly concentric spherical mirrors corrected for all third order aberrations except field curvature. The field curvature is equal to that of a single mirror of the same overall focal length. This 14.265 mm focal length objective is designed to have diffraction limited performance at 0.4 NA and 157 nm wavelength over a 0.5 mm diameter curved field. If flat image surface is used, the useful field size reduces to 0.3 mm diameter.

Figure 2 shows the calculated incoherent square wave modulation transfer function (MTF) over a 0.15 mm radius image field for this objective at 0.4 NA and 157 nm wavelength. The central obscuration in the exit pupil of the system, caused by the primary mirror, reduces the image contrast for objects with middle range spatial frequencies. We define the resolution as the linewidth of a square wave pattern of period which corresponds to spatial frequency in the object (mask) whose incoherent square wave MTF is 0.65. Figure 2 shows that this objective, whose central obscuration is 43%, will have a resolution about 2 times lower than the same system with no obscuration.

In order to avoid obscuration, we used the objective with an eccentric aperture and off-axis illumination as shown in Figure 1. The displacement of the aperture with respect to the optical axis of the objective determines the illumination beam angle, since best imaging requires that the diffraction orders produced by the periodic patterns on the mask be placed symmetrically with respect to the center of the aperture.

The numerical aperture of the system is determined by the aperture stop placed between the mask and the objective as shown in Figure 1. We reduced the numerical aperture from its original value of

Downloaded From: http://spiedigitallibrary.org/ on 03/31/2016 Terms of Use: http://spiedigitallibrary.org/ss/TermsOfUse.aspx

0.4, because had we used this objective at 36 or 14 nm with its full NA, the depth of focus would have been unreasonably short. Another reason for the reducing the NA is to preserve the nearly diffraction limited image quality as the wavelength is reduced. Specifically, the numerical aperture of the system was set to 0.113 at 36 nm and 0.08 at 14 nm. Figure 3 shows the calculated incoherent square wave MTF curves for our objective with the eccentric aperture at both 36 and 13 nm, for a non-symmetric image field of 25 μm $\times$ 50 μm. These MTF curves show the separation of the tangential and sagittal responses which indicates the presence of residual aberrations. Indeed, the lateral shift of the aperture makes the system no longer rotationally symmetric. In such a system, the spherical aberration remains unchanged, but combined with the lateral shift of the aperture generates astigmatism and coma which both are nearly constant over this field.[13] Despite these aberrations, the image contrast is high enough for reasonable imaging in a photoresist.

3. ILLUMINATION

In our experiments we used nearly spatially coherent illumination of the mask, a procedure not normally used in projection lithography. It is well known that images produced with spatially coherent illumination of the mask are characterized by coherent ringing and other unwanted interference. It is possible to have excellent contrast in an image produced with coherent illumination, but with poor fidelity. For example, the concept of depth of focus with coherent illumination is poorly defined, because when the image plane is displaced by $\lambda/(NA)^2$ away from the optimum focus, the features become completely distorted, not just blurred.[14] In addition, the contrast reversal may occur.

In our experiments, the source was not imaged at the entrance pupil of the projection system, defined by the aperture placed in front of the objective. This condition generates non-stationary imaging across the field.[15] This happens because the aperture stop in front of the objective passes different diffraction orders for various points on the mask. As a result, the image of identical features placed at different locations on the mask will vary in the image plane.

Spatially coherent illumination of the small patterned area on the mask makes it necessary to use the eccentric aperture with the objective. If we had used on-axis illumination and a centered aperture, the zero-order (undiffracted light) of the entire pattern and the lower diffraction orders of large features produced by the mask would be blocked by the primary mirror, as shown in Figure 4, resulting in an image similar to that produced in dark field illumination microscopy. In addition, if the system is used with a reflective mask and in the on-axis configuration, the stray light in the system, which can arise from refro-reflections by the mask of the light scattered by the obscuration, may degrade the image contrast.

4. COATINGS

For the experiment at 36 nm the objective mirrors were coated with 17 nm of iridium on top of 6 nm of Cr to provide approximately 8% reflectivity from each mirror surface. For shorter wavelengths the normal incidence reflectivity of all elemental materials falls to less than 1% at 20 nm. Multilayer deposition techniques[16] provide the capability to coat mirror surfaces with materials that can give up to 50% reflectivity at normal incidence for wavelengths as short as 13 nm. For our experiments at 14 nm, the mirrors in the objective were coated with a Mo/Si multilayer. The bilayer spacing (the thickness of Mo/Si pair) in the coatings was optimized to produce the maximum reflectivity at 13.9 nm for the appropriate range of the incidence angles on each mirror. The path of x-rays through the optical system is such that the incidence angles are different on the primary and secondary mirrors, and also vary across the surface of each mirror. Since the spectral response of a multilayer coating depends on the incidence angle, the position of the peak reflectivity varies across the surface of the mirror for a uniform thickness coating. This can be seen in Figure 5, where the calculated reflectance versus wavelength is shown for the primary and secondary mirrors for three

Downloaded From: http://spiedigitallibrary.org/ on 03/31/2016 Terms of Use: http://spiedigitallibrary.org/ss/TermsOfUse.aspx

different rays through the optical system: a central ray and two extreme rays.

Figure 6 shows the spectral response of the Schwarzschild objective. The solid curve is calculated by averaging the product of the primary and secondary mirror reflectances for an ensemble of rays, and also includes the reflections from four Rh-coated beam turning mirrors, the transmission from the Si filter, and the transmission from the Si membrane mask. The measured spectral response of the objective is also shown in Figure 6. These measurements were made by measuring the relative signal from a detector as the incident wavelength was varied. The data are shown with the background subtracted, and with the peak efficiency scaled to coincide with the theoretical peak.

5. EXPERIMENTAL RESULTS

The radiation used in our experiments was obtained from the undulator installed on the U13 beam line at the National Synchrotron Light Source at Brookhaven National Laboratories. Approximately 100 mW of average power at 36 nm in 1% bandwidth was delivered in a 1 mm radius spot at the experiment location. For the 36 nm experiment, the highly collimated beam of radiation was directed to our imaging system with four Si mirrors at 67.5 degrees incidence angle. After passing through a 0.8 μm Al filter, the average power reaching the mask was reduced to roughly 50 μW. (The average power at 14 nm reaching the mask was not measured, but we estimate it to be comparable to the value at 36 nm.)

The design of our projection system permits either a reflection mask or a transmission mask to be used. In our initial experiments we used a transmission mask. However, the ability to use a reflection mask fabricated on a thick, robust substrate, rather than on a thin membrane, is an important advantage of projection lithography over proximity printing.

For 36 nm wavelength exposures we used a free-standing mask fabricated using e-beam lithography and reactive-ion etching to open patterned holes in 0.7 μm thick Si membrane. After creating the pattern, 30 nm of gold was deposited on both sides of the membrane to increase the mask contrast. The pattern was a resolution test chart having both vertical and horizontal lines and spaces ranging in width from 20 μm to 4 μm.

For the 14 nm wavelength experiments we also used a 0.7 μm thick Si membrane, but with a 0.5 μm Ge absorber on it. The absorber was patterned using e-beam direct writing and a tri-level resist. A pattern similar to the free-standing mask but containing features as small as 1 μm was used. Use of a 0.5 μm thick Ge absorber supported on Si membrane permitted the fabrication of smaller features than realized in the free-standing mask, while maintaining a high contrast.

Three electron beam resists were evaluated for exposure at 36 nm using the undulator radiation; they were PBS (polybutene-1 sulfone), EBR-9 (2, 2, 2-trifluoroethyl α-chloro-acrylate), and PMMA (polymethyl methacrylate). The usual resist characteristics, sensitivity and contrast, were obtained by using a stylus profilometer to measure the fraction of resist remaining after development as a function of the logarithm of the exposure dose. For this measurement to yield meaningful results, it is necessary to use thin resist thicknesses to allow the resist to be fully developed away for sufficiently large exposures. Preliminary experiments determined that the depth removed tended to saturate at a value of around 100 nm. Thus, film thicknesses of about 60 nm were used to characterize the resist. The sensitivities of PBS, EBR-9, and PMMA at 36 nm were found to be 0.07, 0.7, and 16 mJ/cm^2, respectively. The contrast of the three resists was determined at 50% residual film thickness to be approximately 1.0 for PBS, 1.5 for EBR-9, and 1.8 for PMMA.

Figure 7 shows a scanning-electron micrograph of a wet-developed image in a 60 nm thick layer of PMMA on silicon; the exposure time was 12 sec. The images of lines and spaces having widths of 1.0, 0.5, 0.38, 0.25 and 0.2 μm are shown as well as the closeup image of 0.2 μm lines and spaces. The structure on the edges of the pattern, including the obvious extra stripe along the edge of the large

Downloaded From: http://spiedigitallibrary.org/ on 03/31/2016 Terms of Use: http://spiedigitallibrary.org/ss/TermsOfUse.aspx

lines, is likely due to the spatial coherence of our illumination.

The high absorption of carbon-based polymers at 36 nm requires that currently available imaging resists be used in thicknesses less than 0.1 μm. Such thin layers are not durable against etchants and thus are not very useful, by themselves, for processing. However, as we demonstrate here, thin layers can be used as the imaging layers in a tri-level resist. This permits the recorded pattern to be transferred by reactive-ion etching into a thick, underlying polymer layer which may then be used for subsequent processing.[17] The tri-level scheme we used is comprised of 60 nm top layer of PMMA, a middle layer of 30 nm Ge, and a bottom layer of 300 nm of hard-baked Shipley 1803 photoresist. After exposure and development of the imaging layer, the pattern is transferred to the middle Ge layer by RIE in SF_6. This layer then serves as an etch mask for RIE of the bottom layer in oxygen. The resulting profile in the bottom resist layer is shown in Figure 8a for the 0.2 μm lines and spaces. The dramatic enhancement in contrast afforded by a tri-level resist may render this imaging technique practical with current technology. To further illustrate this point, Figure 8b show these same tri-level resist patterns etched into the silicon surface using RIE with CF_3Br. The residual photoresist has been removed by oxygen plasma etching.

For our first exposure experiments at 14 nm we used the same tri-level resist scheme; however, because PMMA is less absorptive at this wavelength, we should be able to increase the imaging resist thickness, perhaps in excess of 200 nm. Figure 9a shows an SEM photo of a wet-developed image of 0.1 μm lines and spaces in a 60 nm thick layer of PMMA. Because of the reduced absorption in photoresist at 14 nm, the edge profiles are better than those in PMMA at 36 nm. Figure 9b shows 0.1 μm lines and spaces transferred into the bottom layer of the tri-level resist.

6. CONCLUSION

We have demonstrated reduction projection printing of features as small as 0.1 μm using soft x-ray radiation. The optical system was a Schwarzschild 20$\times$ reduction objective with a 25$\times$50 μm image field. The optical system was fabricated, assembled and aligned at GCA/Tropel, and was used in our imaging experiments with soft x-rays at 36 and 13.9 nm. The use of Mo/Si multilayer coatings at 13.9 nm permitted us to print features as small as 0.1 μm. In our experiments we used transmission masks; however, the design of our projection system permits the use of reflection masks as well. In our initial experiments we used coherent illumination of the mask which provides high contrast images, but accompanied by the edge ringing, speckle, ghost images and other unwanted interferences. At these wavelengths, resist layers must be thin; however, we showed that these thin layers can be used successfully as the imaging layers in a tri-level resist.

7. ACKNOWLEDGEMENT

This work was partially supported by Air Force Office of Scientific Research under Grant #88-0018.

8. REFERENCES

1. V. Pol, J. M. Bennewitz, G. C. Escher, M. Feldman, V. A. Firtion, T. E. Jewell, B. E. Wilcomb, and J. T. Clemens, "Excimer laser-based lithography: a deep ultraviolet wafer stepper," SPIE Proc., vol. 633 (1986).
2. Y. Tanaka, M. Takeda, M. Saito, T. Kasuga and T. Tsumori, "Sub-half micron lithography with excimer laser," SPIE Proc., vol. 1088 (1989).
3. A. Tanimoto, A. Miyaji, Y. Ichihara, T. Uemura, and I. Tanaka, "Excimer laser stepper for sub-half micron lithography," SPIE Proc., vol. 1088 (1989).

Downloaded From: http://spiedigitallibrary.org/ on 03/31/2016 Terms of Use: http://spiedigitallibrary.org/ss/TermsOfUse.aspx

4. L. K. Wang et. al., "Application of synchrotron x-ray lithography to fabricate fully scaled 0.5μm CMOS," J. Vac. Sci. Technol. B 7 (6), 1662 (1989).

5. S. Ishihara, M. Kanai, A. Une, and M. Suzuki, "A vertical stepper for synchrotron x-ray lithography," J. Vac. Sci. Technol. B 7 (6) 1652 (1989).

6. G. Zwicker, W. Windbracke, H. Bernt, D. Friedrich, H.-L. Huber, E. Krullmann, M. Pelka, P. Lange, P. Hemicker, and P. Staudt-Fischbach, "Fabrication of 0.5μm n- and p-type metal-oxide semiconductor test devices using x-ray lithography," J. Vac. Sci. Technol. B 7 (6), 1642 (1989).

7. A. B. C. Walker, R. B. Hoover, T. W. Barbee, Jr., and J. F. Lindbllom, Science (USA) 241, 1781 (1989).

8. See, for example, Y. Vladimirsky, D. Kern, W. Meyer-Ilse, and D. Attwood, Appl. Phys. Lett. 54, 286 (1989); G. Schmahl, D. Rudolph, P. Guttman, and O. Christ, in X-ray Microscopy, Schmahl and Rudolph, ed. (Springer-Verlag, 1983), p.63;
H. Aritome, K. Nagata, and S. Namba, Microelectronic Engineering 3, 459 (1985); and J. A. Trail and R. L. Byer, Opt. Lett. 14, 539 (1989).

9. H. Kinoshita, K. Kurihara, Y. Ishii, and Y. Torii, "Soft x-ray reduction lithography using multilayer mirrors," J. Vac. Sci. Technol. B 7 (6), 1648 (1989).

10. A. M. Hawryluk and L. G. Seppala, "Soft x-ray projection lithography using an x-ray reduction camera," J. Vac. Sci. Technol. B 6, 2162 (1988).

11. W. T. Silfvast and O. R. Wood, II, "Tenth micron lithography with a 10 Hz 37.2 nm sodium laser," Microelectronic Engineering 8, 3 (1988).

12. Tropel Division of GCA Corp.

13. T. E. Jewell "Aberration field properties of simple non-axially symmetric optical systems," M. S. Thesis, University of Arizona (1984).

14. D. S. Goodman, "Lithographic image simulations," paper presented at Microcircuit Engineering 85, Sept. 1985.

15. D. S. Goodman, A. E. Rosenbluth, "Condenser aberrations in Köhler illumination," SPIE Proc., vol. 922 (1988).

16. M. P. Bruijn, J. Verhoeven, E. Puik, and M. J. van der Wiel, "Multilayer X-ray Mirrors: The State of the Art," SPIE Proc. 984 p. 54 (1988).

17. D.M. Tennant, L. D. Jackel, R. E. Howard, E. L. Hu, P. Grabbe, R. J. Capik, B. S. Schneider, "Twenty-five nm features patterned with trilevel e-beam resist," J. Vac. Sci. Technol., 19(4), (1981).

Downloaded From: http://spiedigitallibrary.org/ on 03/31/2016 Terms of Use: http://spiedigitallibrary.org/ss/TermsOfUse.aspx

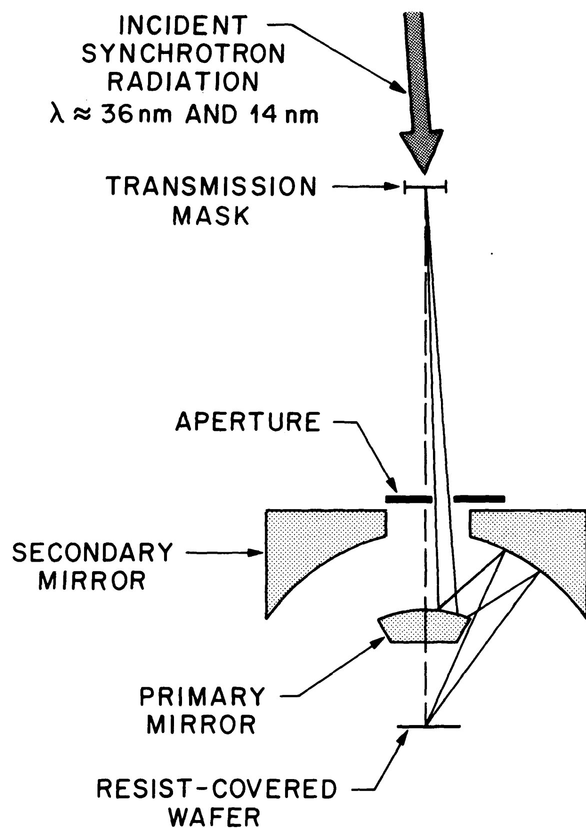

Fig. 1. Schematic diagram showing the Schwarzschild objective used with an eccentric aperture and off-axis illumination.

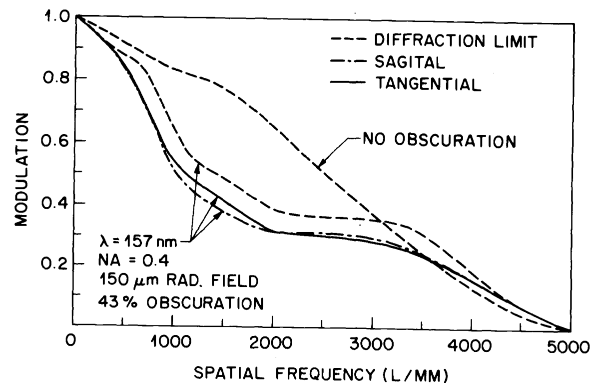

Fig. 2. Calculated incoherent square wave MTF over a 0.15 mm radius image field at 157 nm wavelength and 0.4 NA. The response of the same system with no obscuration is also shown.

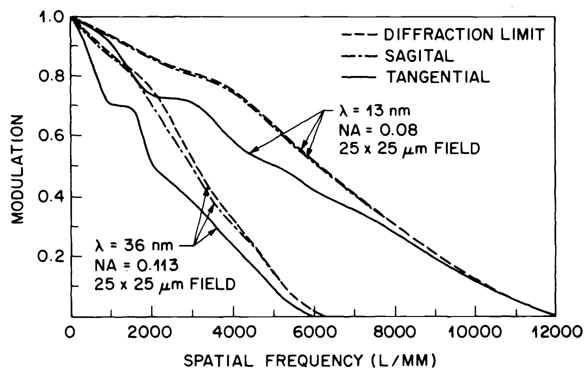

Fig. 3. Calculated incoherent square wave MTF for the objective used with the eccentric aperture at 36 and 13 nm.

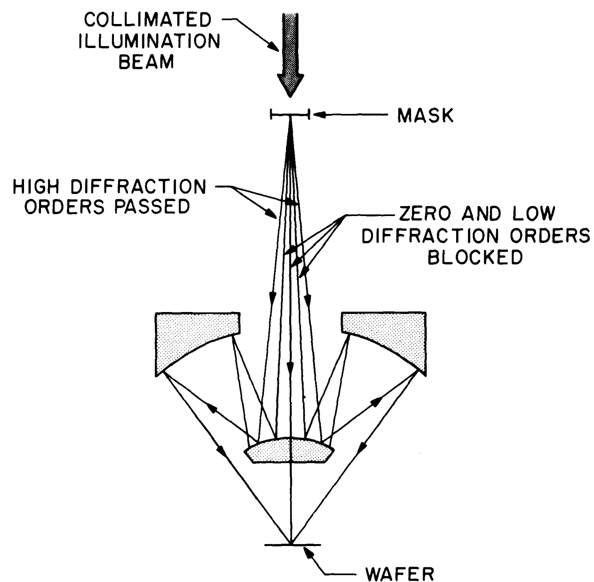

Fig. 4. Schematic diagram showing the objective used at full aperture and with axial illumination, where zero and lower diffraction orders are blocked.

Downloaded From: http://spiedigitallibrary.org/ on 03/31/2016 Terms of Use: http://spiedigitallibrary.org/ss/TermsOfUse.aspx

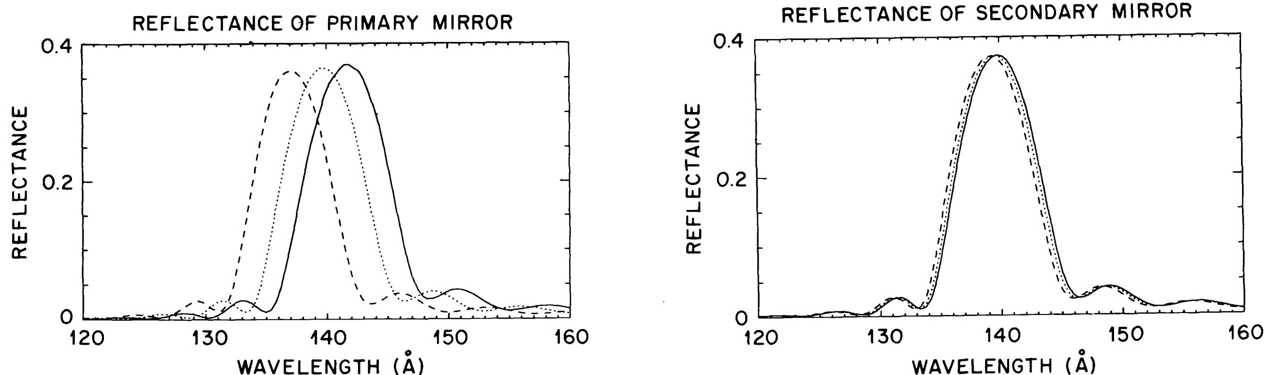

Fig.5.Calculated reflectance versus wavelength for the primary and secondary mirrors for different incidence rays. For the primary (secondary) mirror corresponding incidence angles are: solid - 9.8°(3.5°); dashed - 13.7°(4.6°); dot-dashed - 17.5° (6.2°).

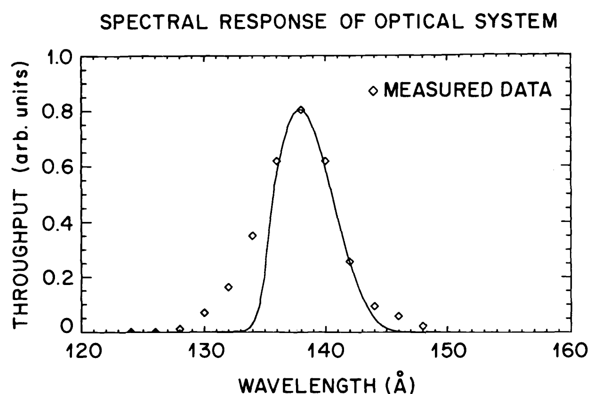

Fig. 6. Relative throughput of the experimental system at 14 nm, including reflections in the objective, beam turning mirrors, and transmission of Si filter and Si membrane mask. Measured data are also shown.

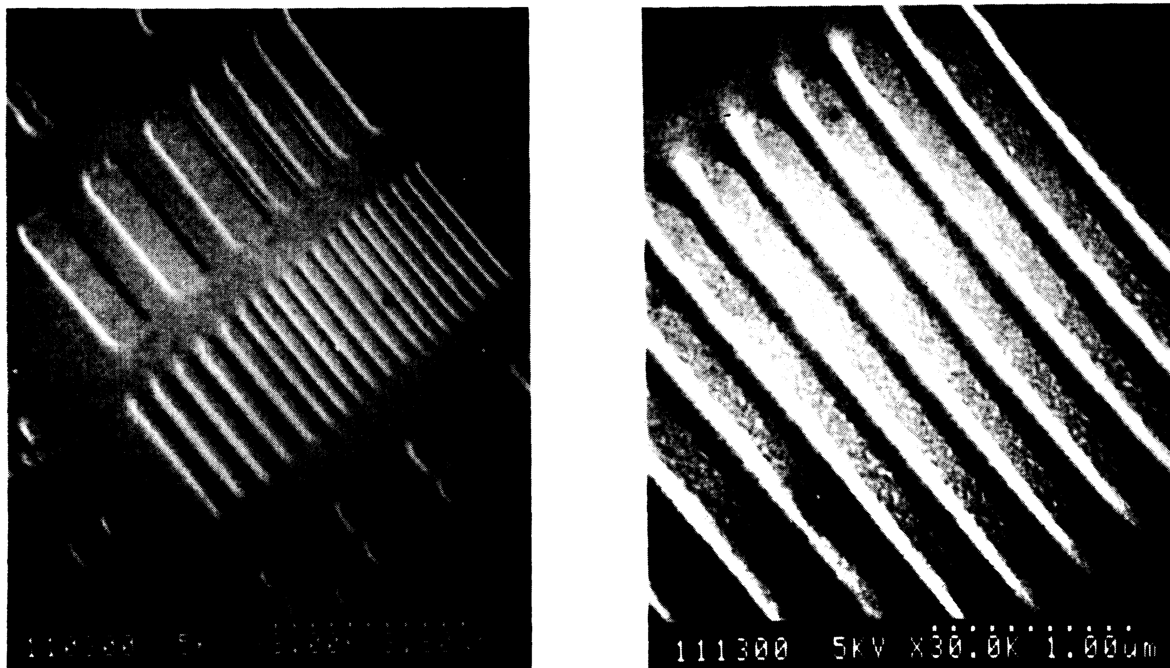

Fig. 7. Left: SEM micrographs of developed images in 60 nm thick film of PMMA on silicon. Lines and spaces shown have widths of 1, 0.5, 0.375, 0.25, and 0.2 μm. Right: a closeup image of the 0.2 μm lines and spaces.

Downloaded From: http://spiedigitallibrary.org/ on 03/31/2016 Terms of Use: http://spiedigitallibrary.org/ss/TermsOfUse.aspx

Fig.8a. SEM photo of 0.2 μm lines and spaces transferred from the imaging layer into the bottom resist layer.

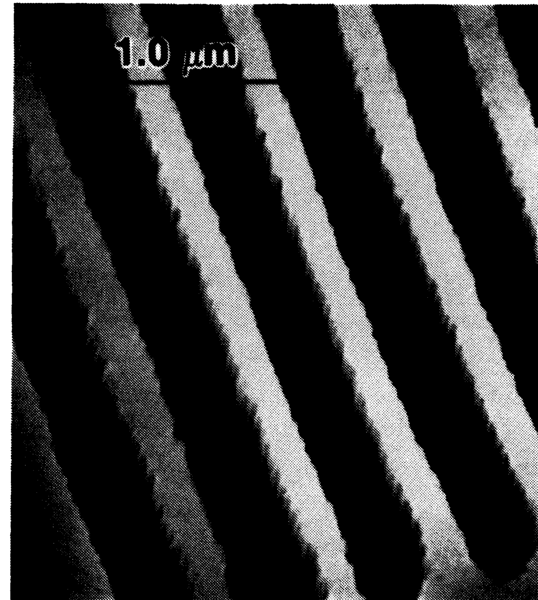

Fig.8b. 0.2 μm lines and spaces transferred into the silicon wafer.

Fig.9a. SEM photo of the wet-developed image of 0.1 μm lines and spaces in 60 nm thick layer of PMMA.

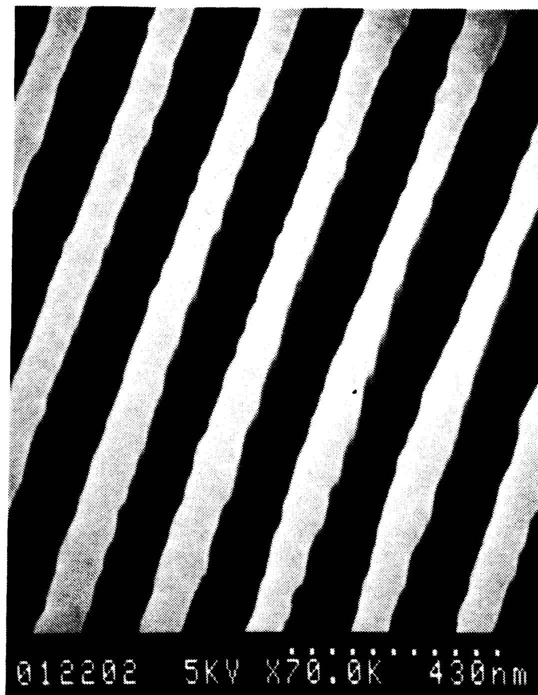

Fif.9b. 0.1 μm lines and spaces transferred into the bottom layer of a tri-level resist.

Downloaded From: http://spiedigitallibrary.org/ on 03/31/2016 Terms of Use: http://spiedigitallibrary.org/ss/TermsOfUse.aspx